PNAS
www.pnas.org

Supplementary Information for

Spatially resolved metabolomics to discover tumor-associated metabolic alterations

Chenglong Sun, Tiegang Li, Xiaowei Song, Luojiao Huang, Qingce Zang, Jing Xu, Nan Bi, Guanggen Jiao, Yanzeng Hao, Yanhua Chen, Ruiping Zhang, Zhigang Luo, Xin Li, Luhua Wang, Zhonghua Wang, Yongmei Song, Jiuming He and Zeper Abliz

Jiuming He and Zeper Abliz

Email: hejiuming@imm.ac.cn; zeper@imm.ac.cn

This PDF file includes:

Supplementary text
Figs. S1 to S38
Tables S1 to S2
References for SI reference citations

www.pnas.org/cgi/doi/10.1073/pnas.1808950115

Supplementary Information Text

Solvents and Reagents. HPLC-grade acetonitrile (ACN) was purchased from Merck (Muskegon, USA). Triton X-100 and paraformaldehyde were obtained from solarbio (Beijing, China). Bovine Serum Albumin (BSA) was provided by sigma (St. Louis, USA). TWEEN 20 was obtained from VWR LIFE SCIENCE (Radnor, PA, USA). PV-9000 two-step immunohistochemical kit, DAB kit, haematoxylin and eosin were provided by Beijing Zhongshan Goldenbridge Biotechnology Company (Beijing, China). Ethanol, xylene and hydrochloric acid were purchased from Beijing Chemical Works (Beijing, China). Purified water was obtained from Wahaha (Hangzhou, China).

AFADESI-MSI analysis. A home-built AFADESI ion source was installed on Q-Qrbitrap mass spectrometer (Q Exactive, Thermo Scientific Bremen, Germany) after remove the original ion sourc. 3D translational stage controlled by custom-developed software was placed under the ion source. SC100 series stepper motor (Beijing Optical Century Instrument Co., Beijng, China) was used to control the 3D mobile platform.

Screening of discriminant *m/z* features. After tissue metabolite imaging (Fig. S21 *A*), we import histology image to the custom-developed mass spectrometry imaging software (Fig. S21 *B*), which facilitates the overlay of histology and MS images (Fig. S21 *C*). Then, the overlay images help to extract region-specific mass spectra (Fig. S21 *D*). Next, the spatially-resolved mass spectra can be used to perform *in situ* PLS-DA analysis. Meanwhile, the classification loading values of each *m/z* were given according to their discrimination ability (Fig. S21 *E*). Then, we screened the significantly discriminant *m/z* features by construction the MS images of the ions with large classification loading values (Fig. S21 *F*).

Immunohistochemistry. The expression of PYCR2, GLS, FASN, UPase1, HDC and ODC in ESCC tissues was assessed by immunohistochemical staining using specific antibodies. Successive frozen tissue sections, which were adjacent to the section analyzed by AFADESI-MSI, were warmed at room temperature for 20 min. The sections were fixed in paraformaldehyde for 10 min. After washing in PBS, the sections were immersed in 0.25% Triton X-100 for 15 min to make the tissue permeable and then blocked with 1% bovine serum albumin (BSA) for 30 min at room temperature. The sections were incubated with antibodies against PYCR2 (Abcam; ab185578; 1:300), GLS (Abcam; ab156876; 1:250), FASN (Abcam; ab128870; 1:300), UPase1 (Abcam; ab205031; 1:150), HDC (Abcam; ab37291; 1:150), and ODC (Abcam; ab66067; 1:350) at 4 °C overnight, followed by rewarming at room temperature for 20 min. Then, a PV-9000 two-step immunohistochemical kit was used according to the manufacturer's instructions, and a DAB kit was used subsequently to detect antigen-antibody binding (all from Zhongshan Goldenbridge Biotechnology Ltd. Co., Beijing, China). Slides were then counterstained using hematoxylin, dehydrated, mounted and covered. Images were visualized by a Pannoramic MIDI scanner (3DHISTECH, Budapest, Hungary) and analyzed by Image-Pro Plus (IPP, version 6.0, Silver Spring, MD, USA). All IHC photographs were analyzed by using Image ProPlus (IPP, version 6.0, Media Cybernetics, Silver Spring, MD, USA) as described previously (1).

***In situ* AFADESI-MS/MS analysis.** The resolving power was set at 17500 for MS/MS acquisition with the AGC value at 3E6 and maximum injection time at 200 ms. The ions of interest were listed as the targets, with the NCE value set at 25%, 35%, and 45% in targeted-MS2 scan mode. Representative results were shown in Supplementary Figs. S22-S38.

Figures

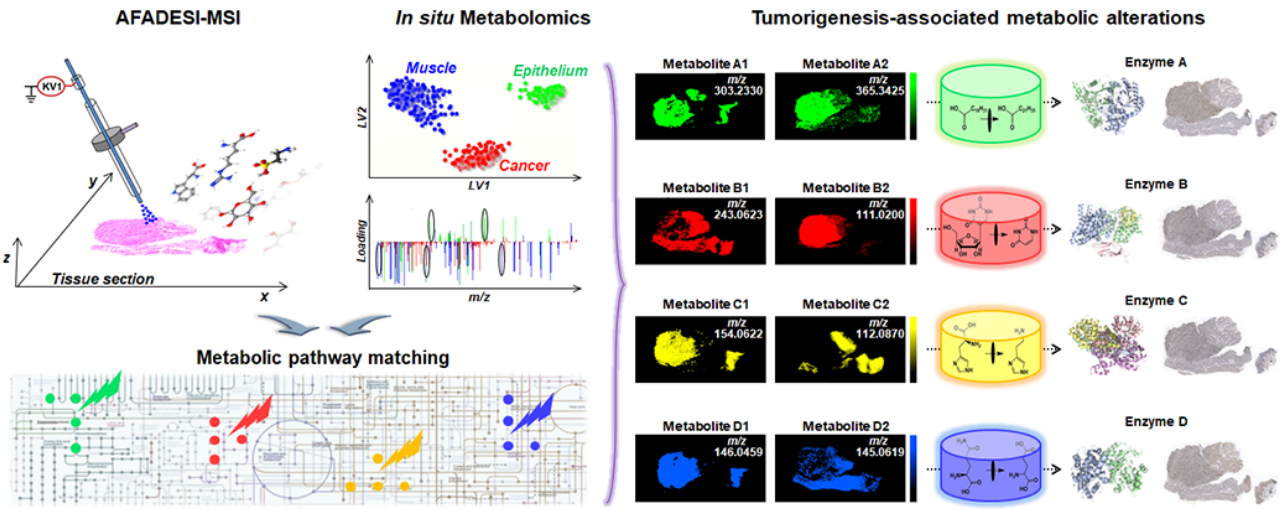

Fig. S1. Strategy for the discovery of tumor-associated metabolic alterations.

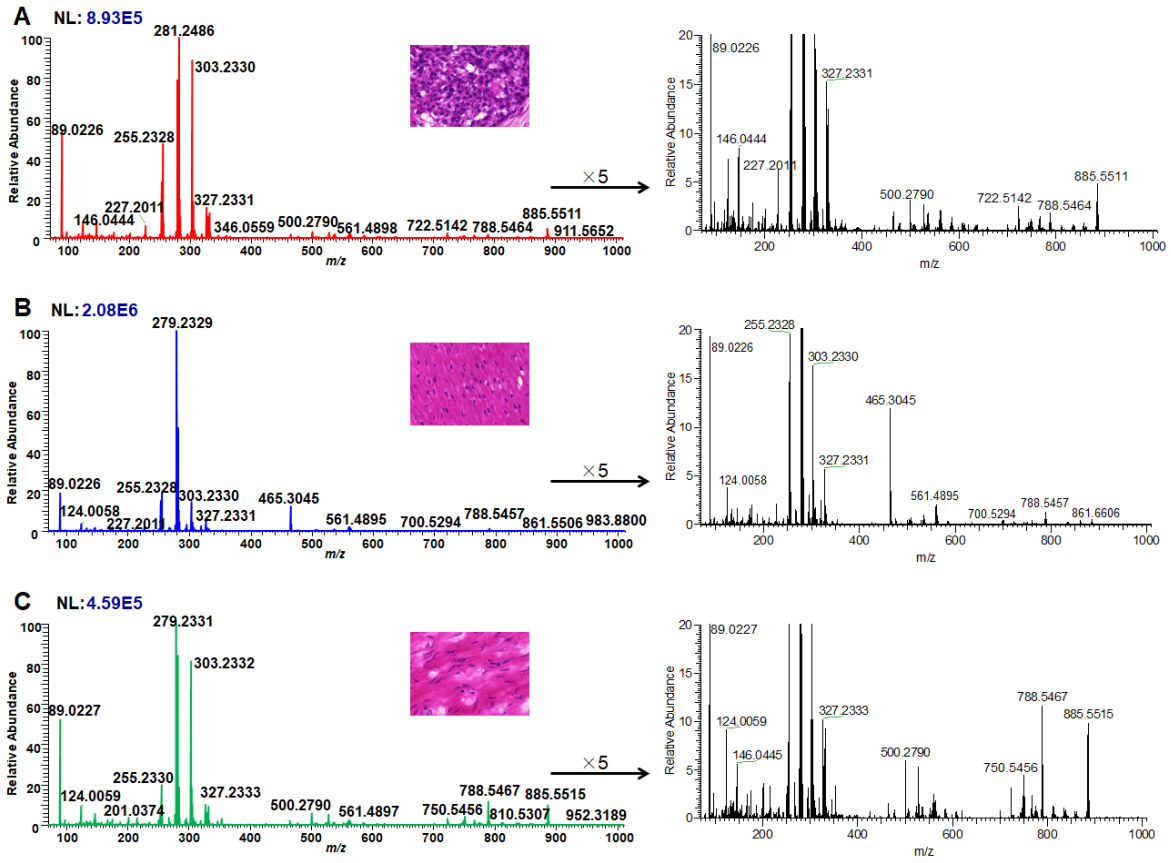

Fig. S2. Representative mass spectra of ESCC related tissues in negative ion mode. (A) Cancer tissue. (B) Epithelial tissue. (C) Muscular tissue.

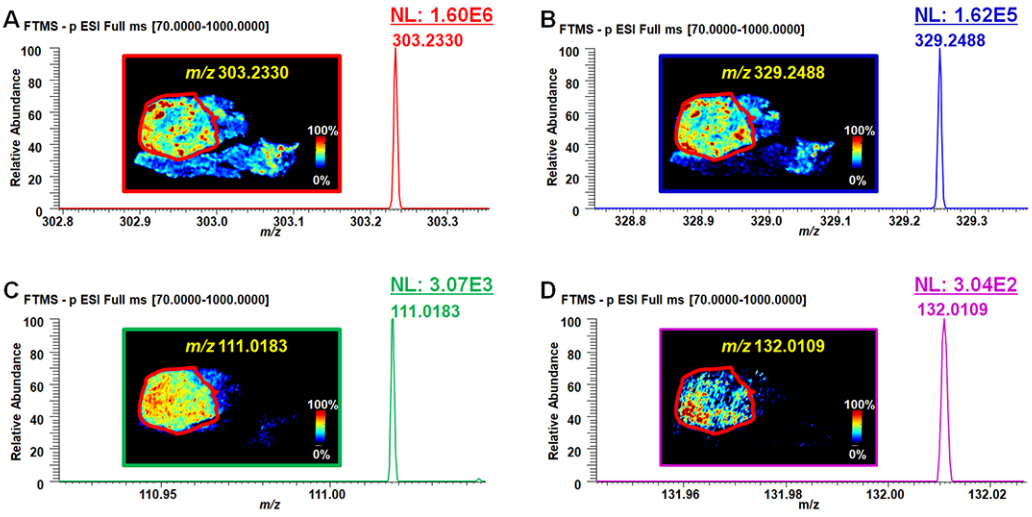

Fig. S3. Content variation of different metabolites in ESCC tissue. Different endogenous metabolites in ESCC tissue section presented a significant content variation, and some even exceed 5,000 folds. (For example, the ion intensity of *m/z* 303.2330 (A) is exceed 5,000 folds than *m/z* 132.0109 (D)).

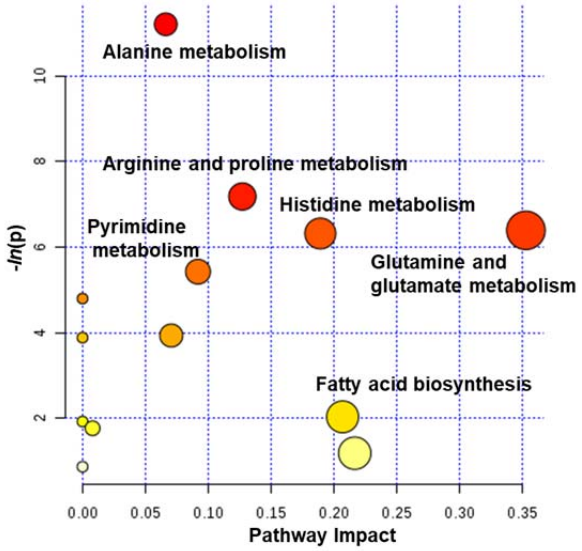

Fig. S4. Metabolic pathway analysis for esophageal cancer.

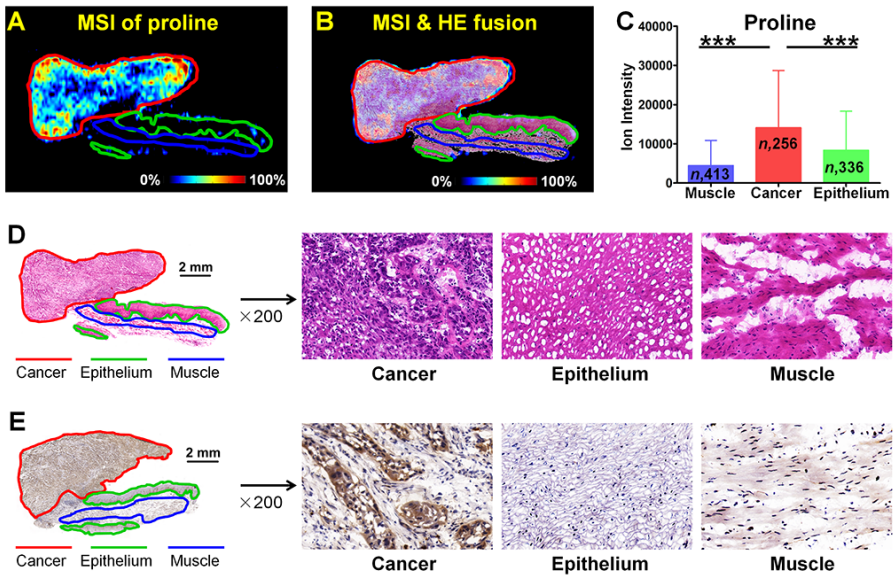

Fig. S5. *In situ* visualization of crucial metabolite and metabolic enzyme in the proline biosynthesis pathway. (A) MS image of proline. (B) MSI & (H&E) overlay image. (C) Proline levels in cancer and paired epithelium and muscle tissues from 256 ESSC patients, ***p<0.001. (D) H&E image of ESCC tissue section. (E) Expression of PYCR2 in different regions of ESCC tissue section.

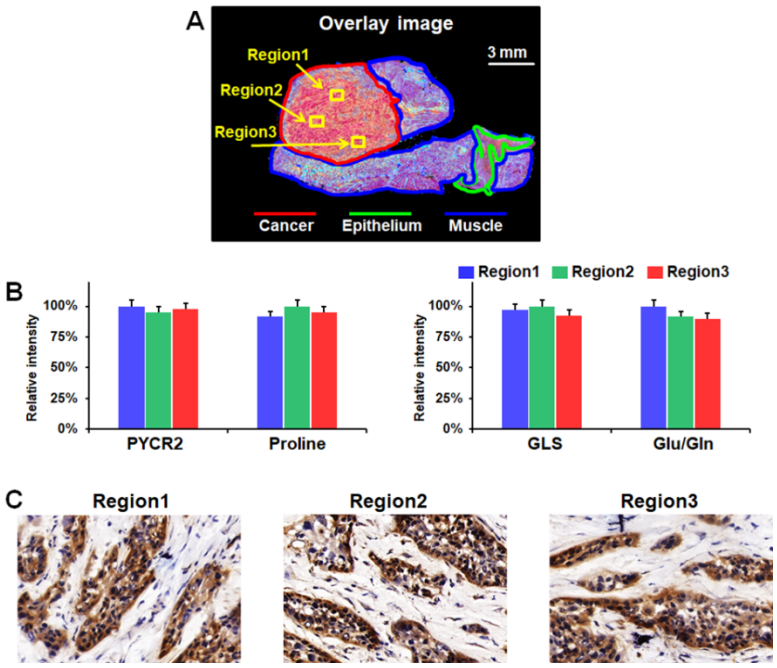

Fig. S6. The spatial distribution of metabolites and corresponding enzymes within a tumor. (A) Microscopy-MSI overlay image and the selection of different regions in a tumor. (B) The expression of PYCR2 and proline, GLS and glutamate (Glu)/glutamine (Gln) in different regions of a tumor section. (C) Representative IHC staining of PYCR2 in different regions of a tumor section (200 ×).

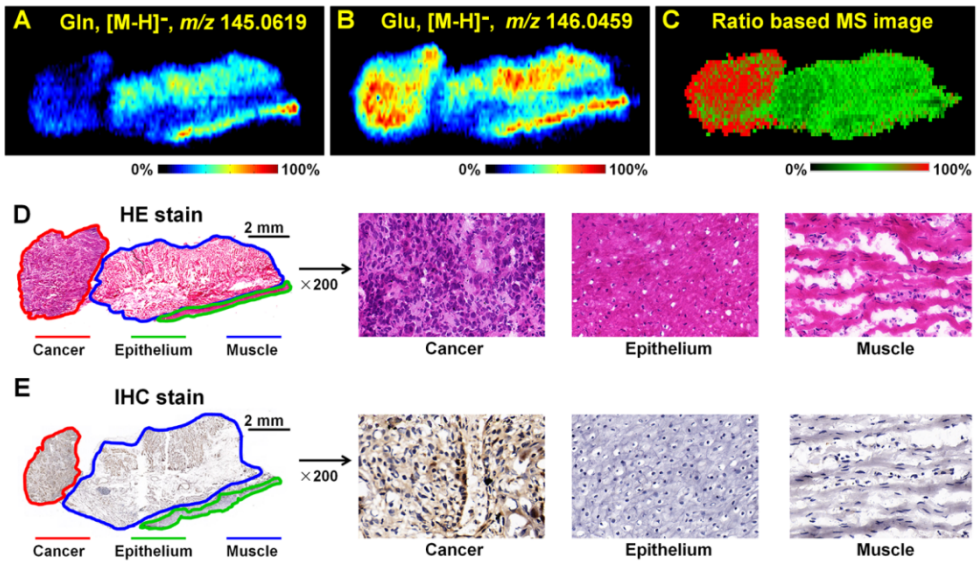

Fig. S7. *In situ* visualization of crucial metabolites and metabolic enzyme in the glutamine metabolism pathway. (A/B) MS images of glutamine (Gln) and glutamate (Glu). (C) The new reconstructed MS image based on ion intensity ratio of Glu to Gln. (D) H&E image of ESSC tissue section. (E) Expression of GLS in different regions of ESSC tissue section.

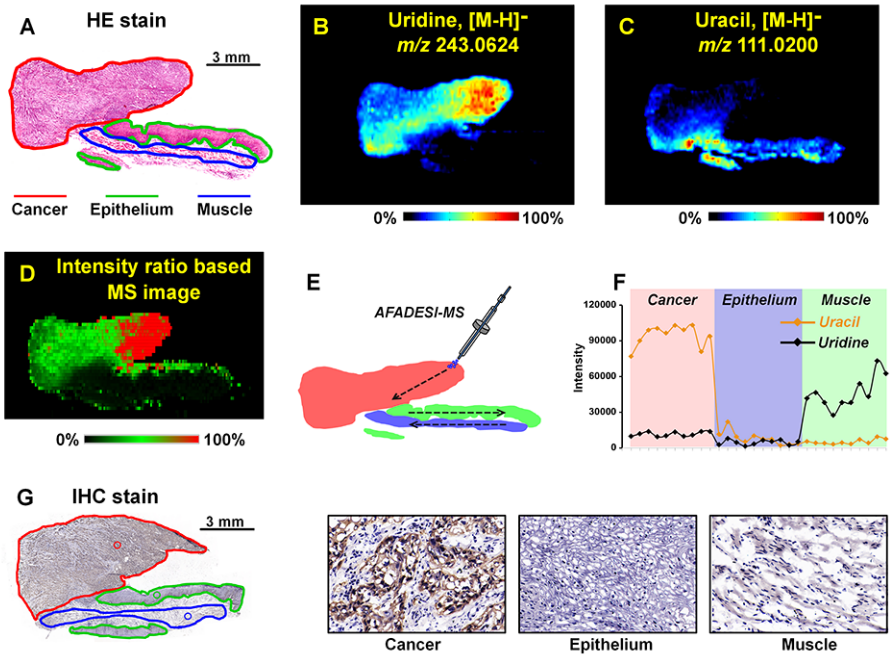

Fig. S8. *In situ* visualization of crucial metabolites and metabolic enzyme in the uridine metabolism pathway. (A) H&E image of ESSC tissue section. (B/C) MS images of uridine and uracil. (D) The new constructed MS image based on ion intensity ratio of uracil to uridine. (E) Scanning-path of AFADESI-MSI. (F) Plot of intensity change of uridine and uracil occurring with the transition from cancer, epithelium to muscle. (G) Expression of UPase1 in different regions of ESSC tissue section.

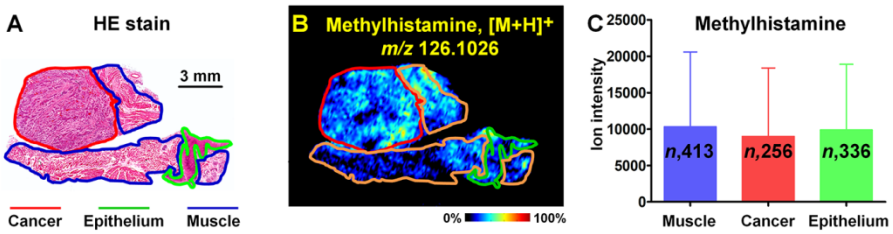

Fig. S9. MS image and statistical result of methylhistamine in ESSC tissue. (A) The H&E image of ESSC tissue section. (B) MS image of methylhistamine in ESSC tissue section. (C) Methylhistamine levels in cancer and paired epithelium and muscle tissues from 256 ESSC patients.

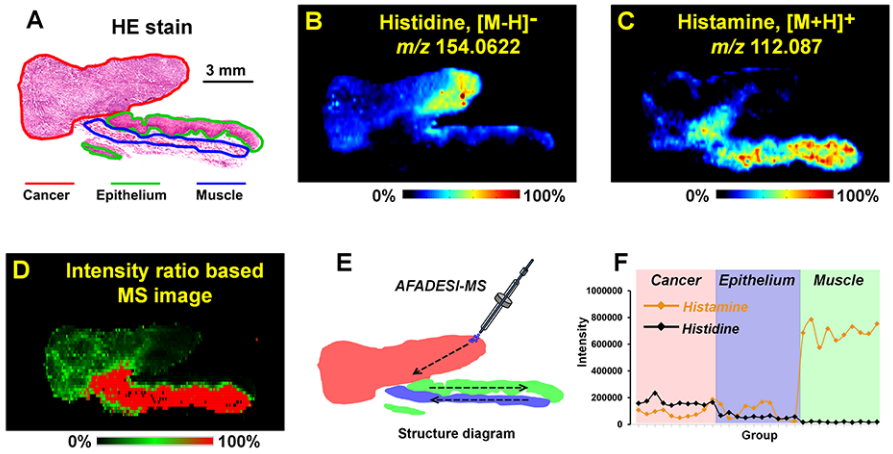

Fig. S10. *In situ* visualization of crucial metabolites in the histamine metabolism pathway. (A) Representative H&E image of ESSC tissue section. (B/C) MS images of histidine and histamine. (D) The new reconstructed MS image based on ion intensity ratio of histamine to histidine. (E) Scanning-path of AFADESI-MSI. (F) Plot of intensity change of histidine and histamine occurring with the transition from cancer, epithelium to muscle.

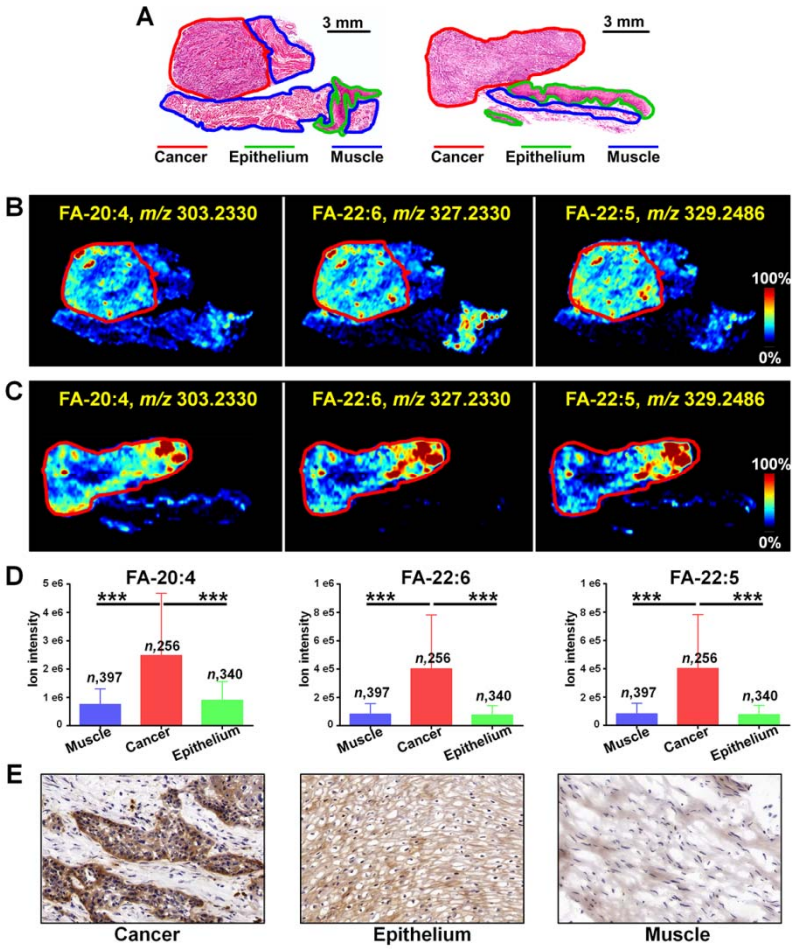

Fig. S11. *In situ* visualization of crucial metabolites and metabolic enzyme in the fatty acids biosynthesis pathway. (A) H&E image of ESSC tissue section. (B/C) MS images of FA-20:4/ FA-22:6/ FA-22:5 in ESSC tissue section. (D) FA-20:4, FA-22:6, and FA-22:5 levels in cancer and paired epithelium and muscle tissues from 256 ESSC patients, ***p<0.001. (E) Expression of FASN in different regions of ESSC tissue section.

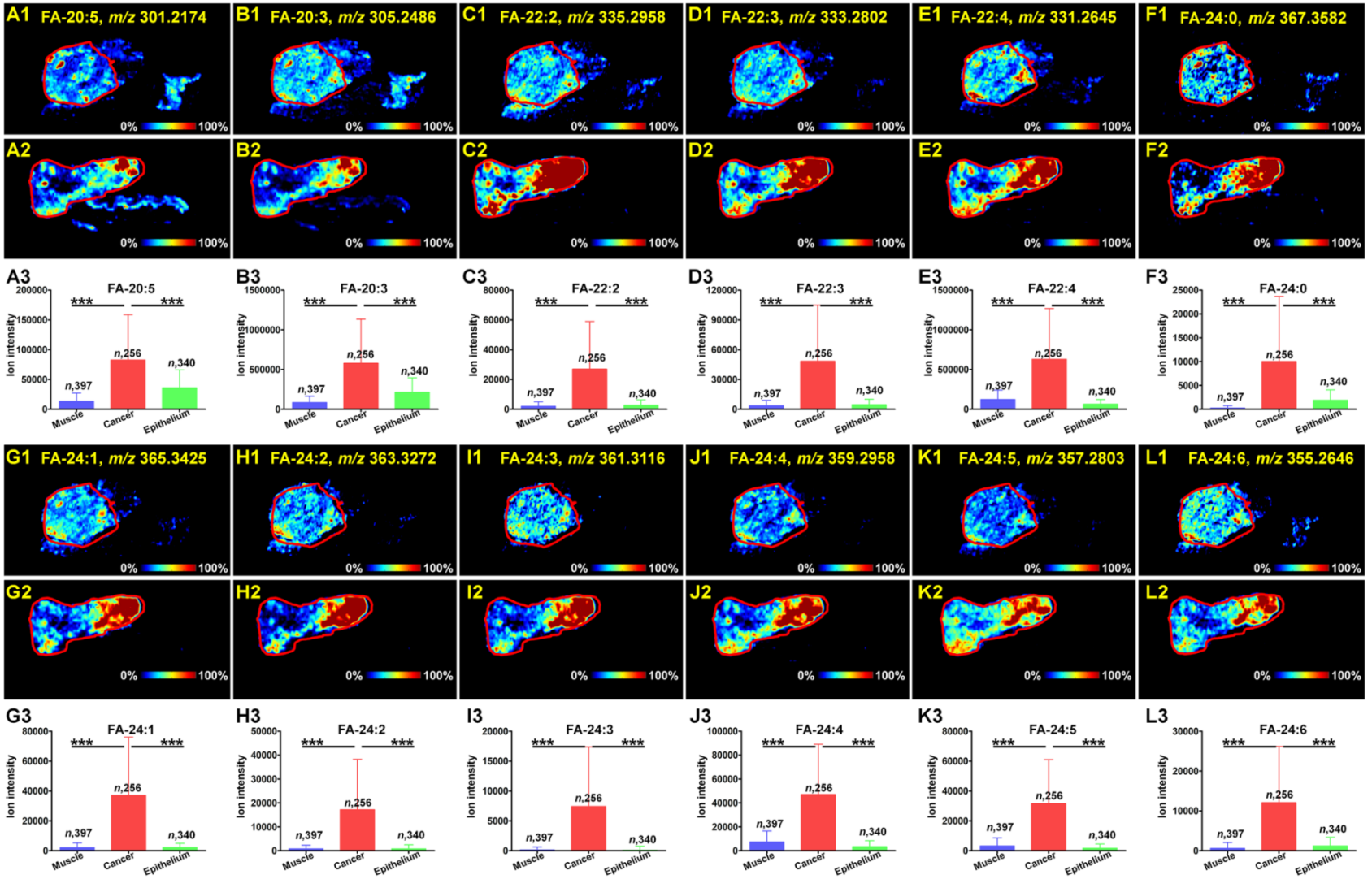

Figure S12. The MS images and statistical analysis of representative fatty acids in ESSC tissue.

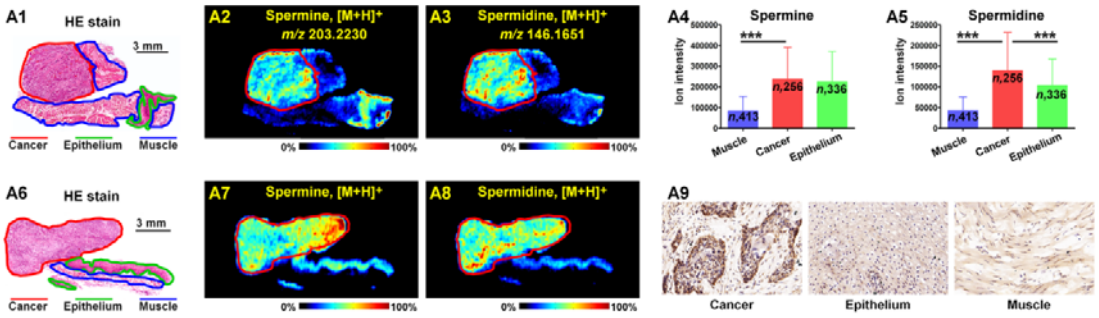

Fig. S13. *In situ* visualization of crucial metabolites and metabolic enzyme in the polyamines biosynthesis pathway. Representative H&E image, MS image and immunohistochemical image of ESSC tissue sections. (A1/A6) Representative H&E image of ESSC tissue section. (A2/A7) MS images of spermine. (A3/A8) MS images of spermidine. (A4) Spermine levels in cancer and paired epithelium and muscle tissues from 256 ESSC patients. (A5) Spermidine levels in cancer and paired epithelium and muscle tissues from 256 ESSC patients. (A9) Expression of ODC in different regions of ESSC tissue section.

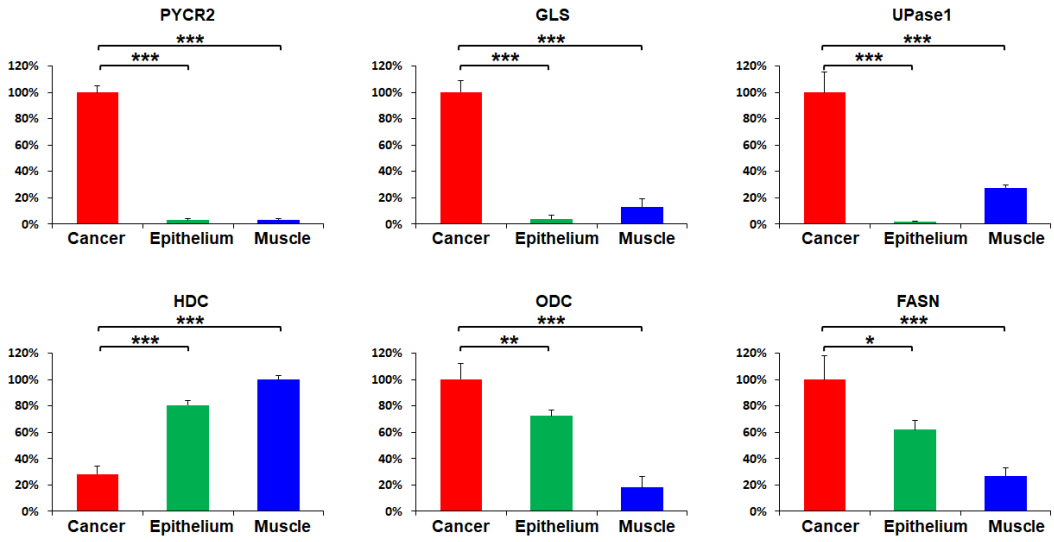

Fig. S14. Columns of the relative mean optical density of PYCR2, GLS, Upase1, HDC, ODC, and FASN expression. The expression of six enzymes in the cancerous area and the normal area are shown as mean + standard deviation (*, $p < 0.05$; **, $p < 0.01$; ***, $p < 0.001$). All IHC photographs were analyzed by using Image ProPlus (IPP, version 6.0, Media Cybernetics, Silver Spring, MD, USA).

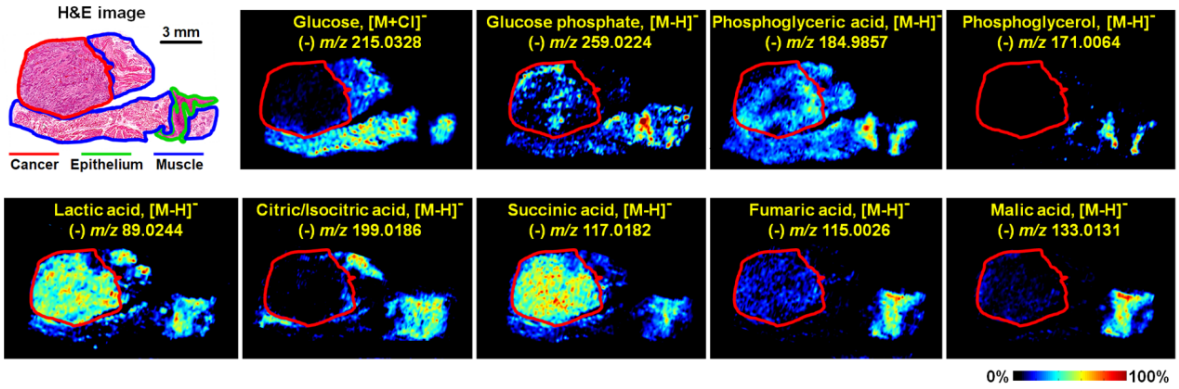

Fig. S15. MS images of representative metabolites in glycolysis metabolic pathway and tricarboxylic acid cycle metabolic pathway.

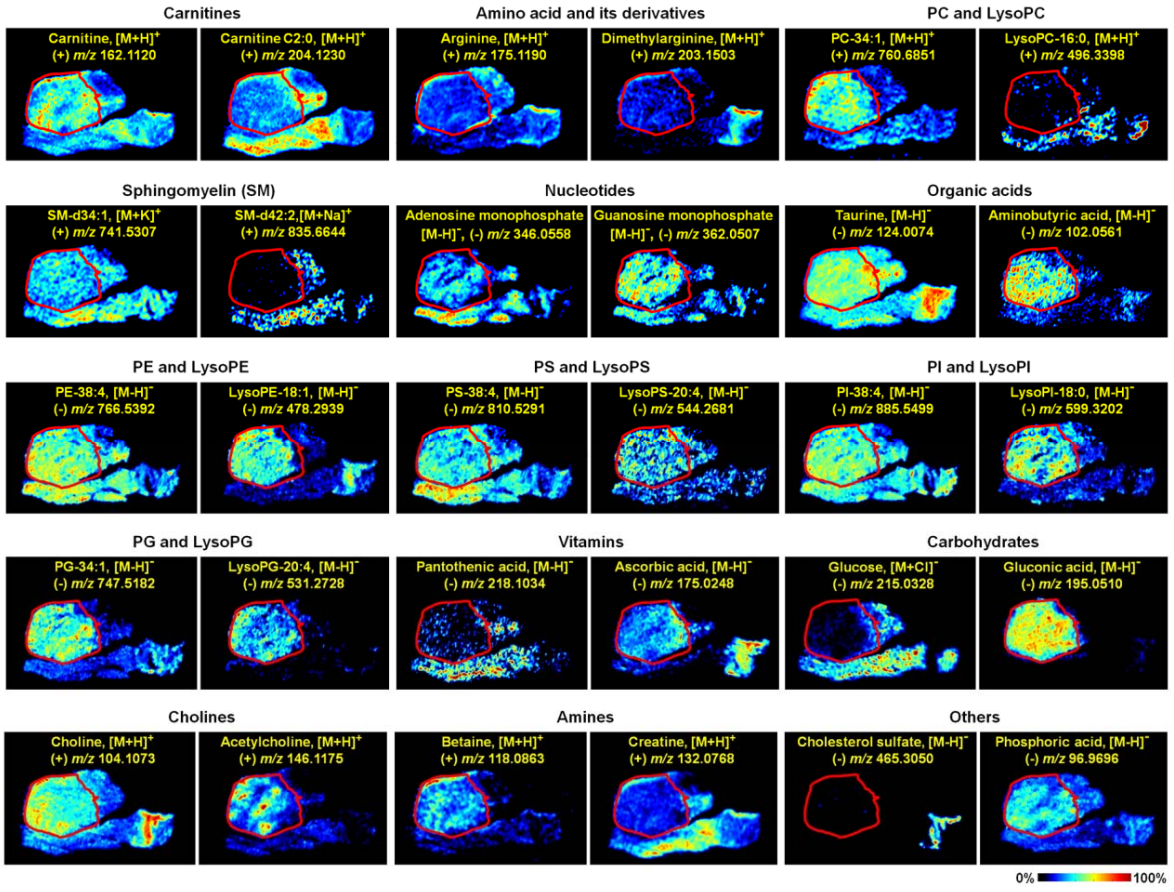

Fig. S16. MS images of different kinds of metabolites in esophageal cancer tissue. PC: Phosphatidylcholine, PI: Phosphatidylinositol, PE: Phosphatidylethanolamine, PS: Phosphatidylserine, PG: Phosphatidylglycerol.

		Numbers	Accuracy	Output: Epithelium	Output: Muscle	Output: Cancer
Input	Epithelium	26	92.3%	24	0	2
	Muscle	28	92.9%	0	26	2
	Cancer	36	97.2%	1	0	35
	Total	90	94.4%	25	26	39

Figure S17. The confusion matrix of the negative PLS-DA model showing classification results of new collected esophageal cancer tissue samples.

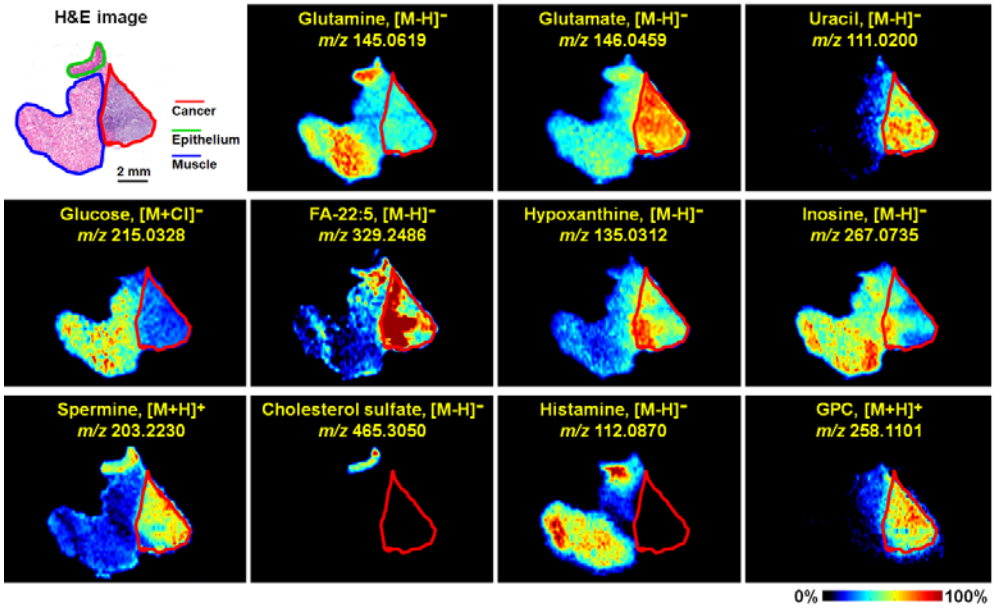

Figure S18. MS images of representative discriminant metabolites of new collected esophageal cancer tissue sample. GPC: Glycerophosphorylcholine, FA: Fatty acid.

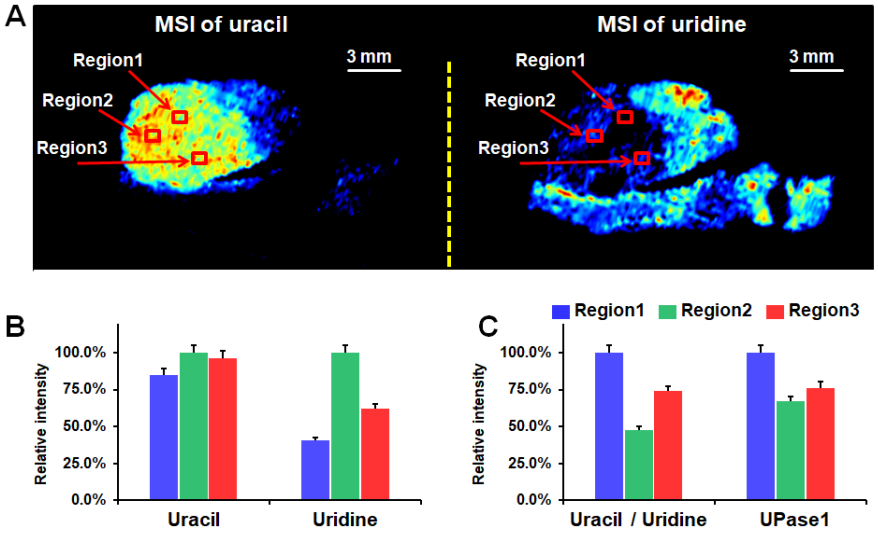

Figure S19. (A) MS images of uracil and uridine. (B) The expression of uracil and uridine in different regions of a tumor section. (C) The intensity ratio of uracil to uridine, and the expression of UPase1 in different regions of a tumor section.

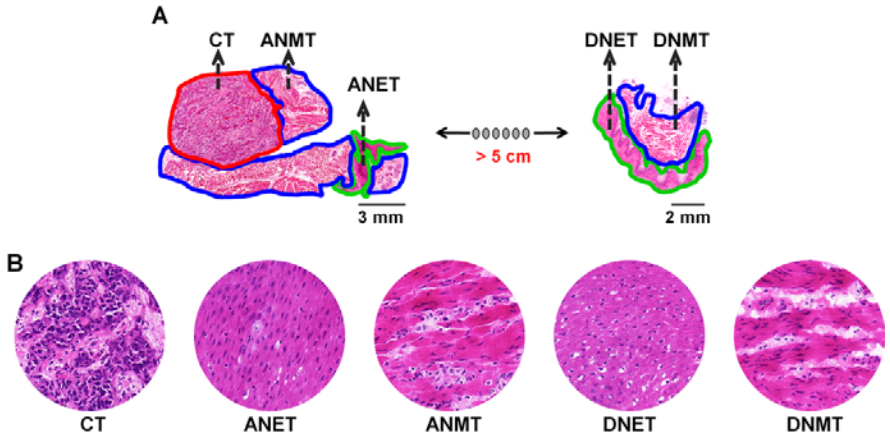

Figure S20. (A) H&E stains of esophageal cancer tissue (CT), adjacent noncancerous tissue (ANT), and distal noncancerous tissue (DNT). (B) ×200 magnified H&E stains. ANET, adjacent noncancerous epithelium tissue; ANMT, adjacent noncancerous muscle tissue; DNET, distal noncancerous epithelium tissue; DNMT, distal noncancerous muscle tissue.

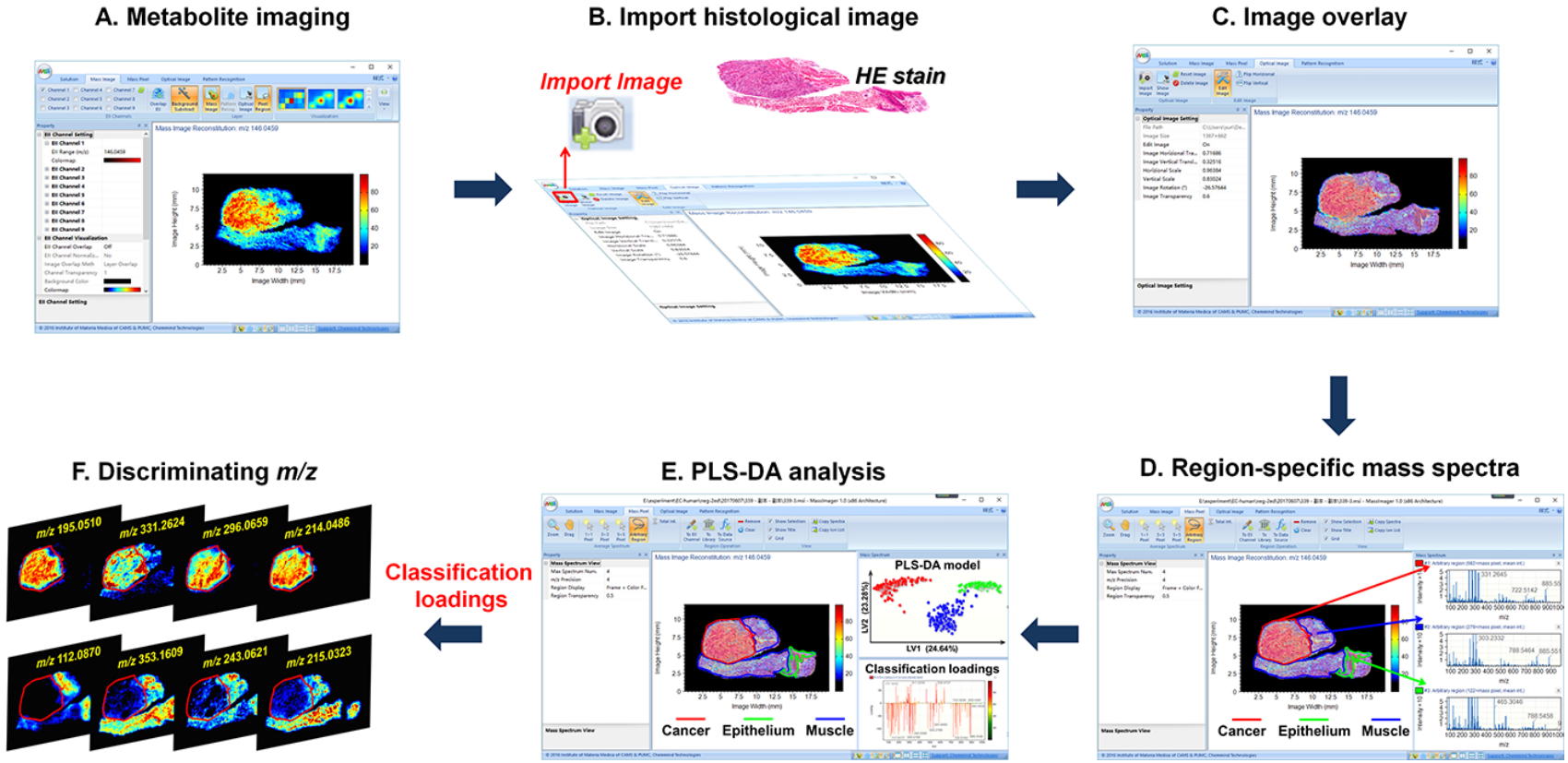

Figure S21. The detailed process of screening significantly discriminant *m/z* features. (A) MS image construction by custom-developed mass spectrometry imaging software; (B) Import histological image into the mass spectrometry imaging software; (C) MS image construction by custom-developed mass spectrometry imaging software; (D) Region-specific mass spectra extraction; (E) PLS-DA analysis based on region-specific mass spectra; (F) Screened discriminating *m/z* based on classification loadings.

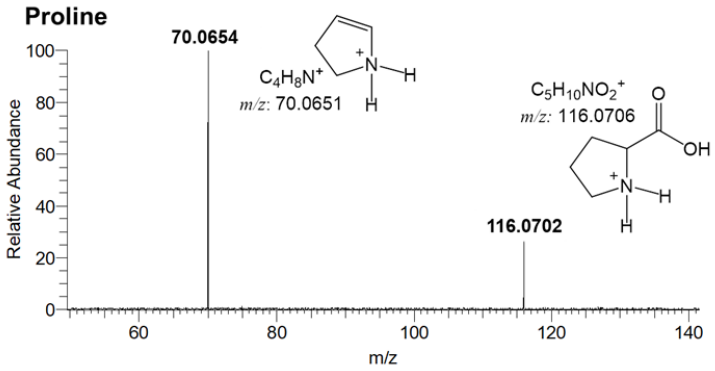

Figure S22. The MS/MS spectrum and the fragmentation pathway of proline.

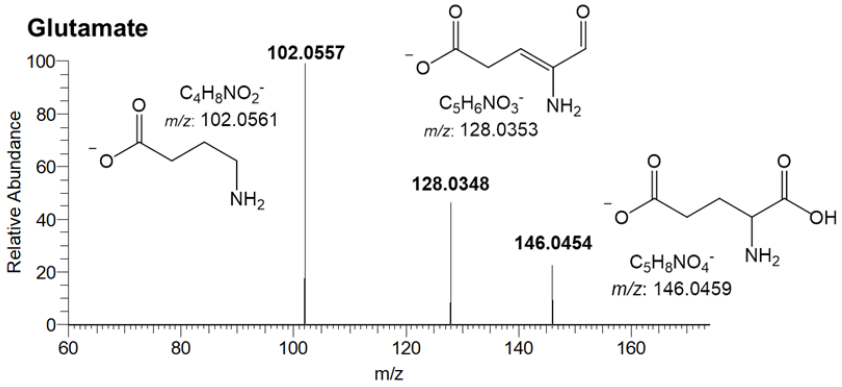

Figure S23. The MS/MS spectrum and the fragmentation pathway of glutamate.

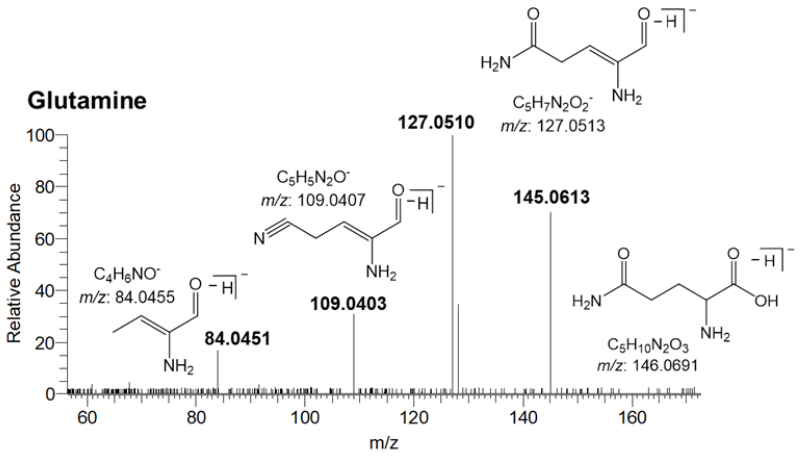

Figure S24. The MS/MS spectrum and the fragmentation pathway of glutamine.

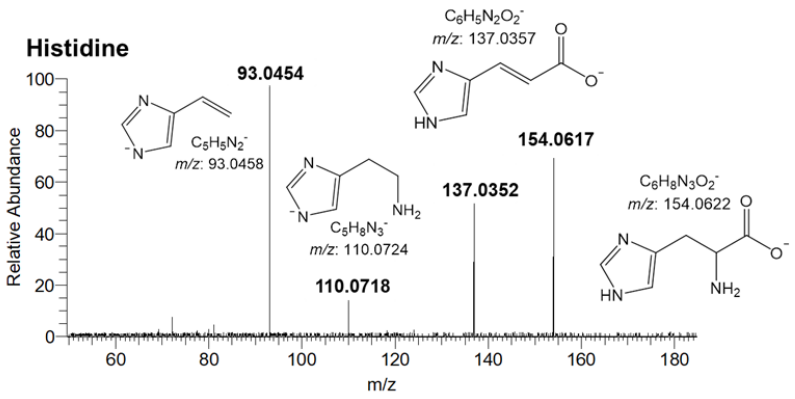

Figure S25. The MS/MS spectrum and the fragmentation pathway of histidine.

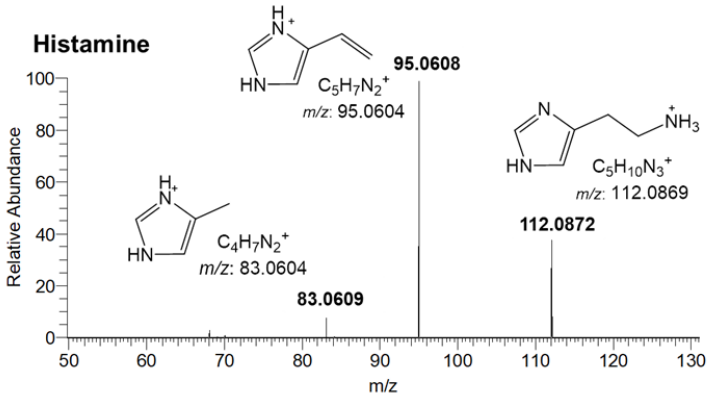

Figure S26. The MS/MS spectrum and the fragmentation pathway of histamine.

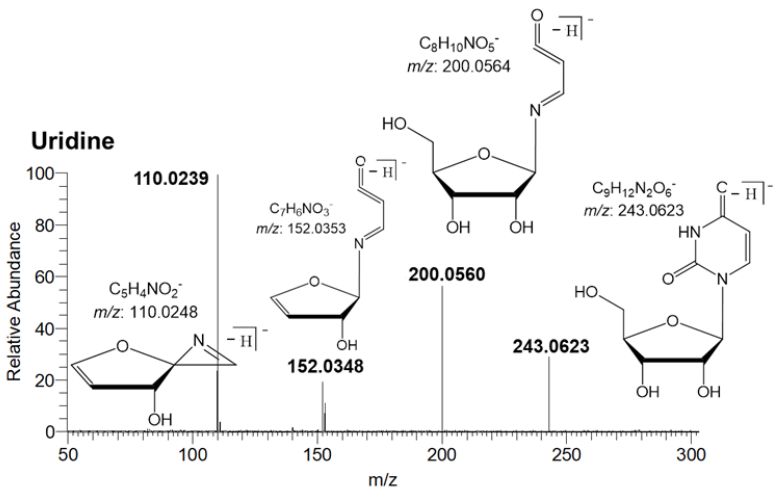

Figure S27. The MS/MS spectrum and the fragmentation pathway of uridine.

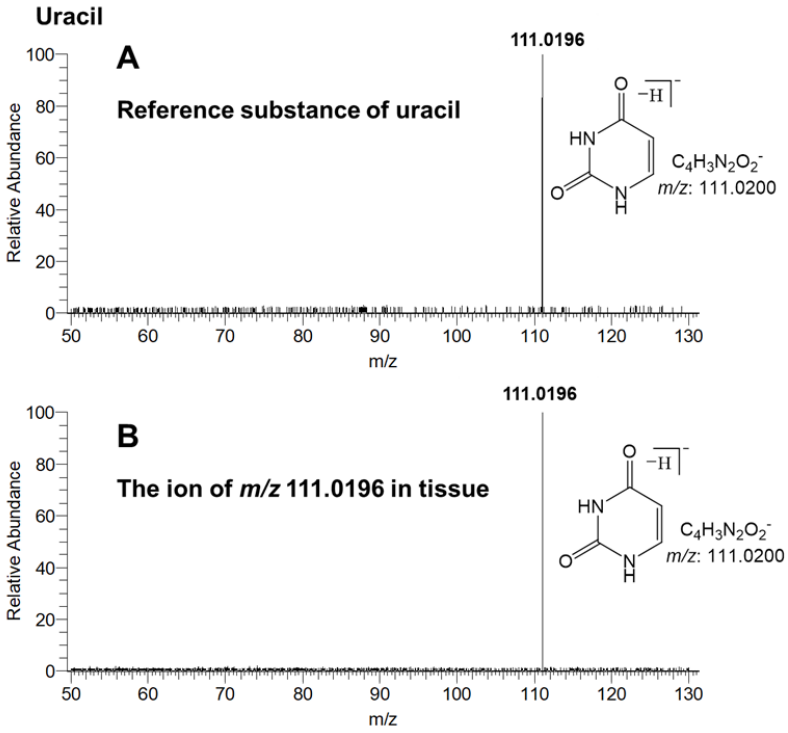

Figure S28. The MS/MS spectrum reference substance of uracil and the ion of *m/z* 111.0196 in cancer tissue.

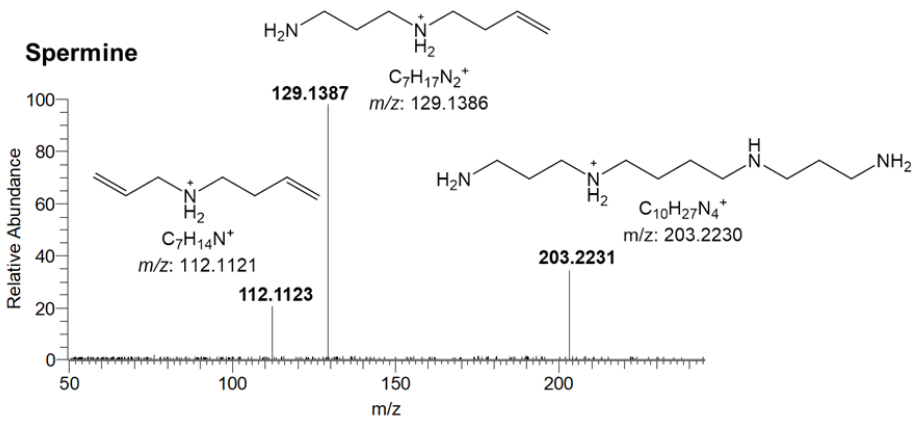

Figure S29. The MS/MS spectrum and the fragmentation pathway of spermine.

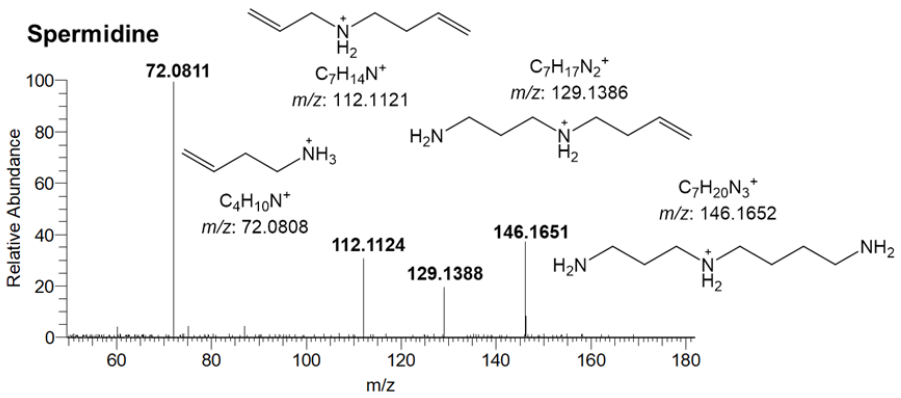

Figure S30. The MS/MS spectrum and the fragmentation pathway of sperdimine.

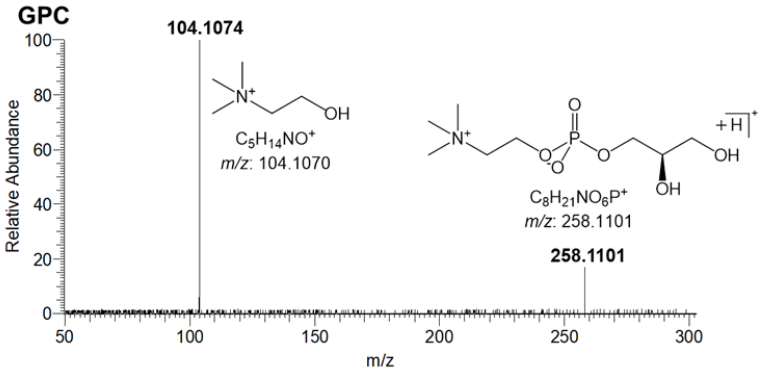

Figure S31. The MS/MS spectrum and the fragmentation pathway of GPC (glycerophosphoryl choline).

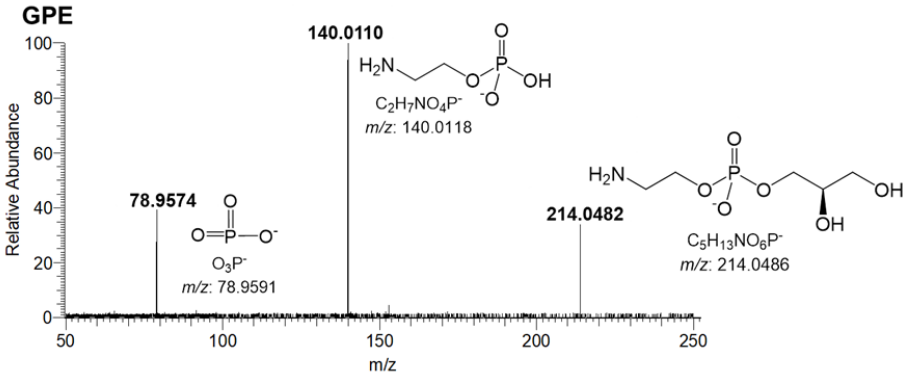

Figure S32. The MS/MS spectrum and the fragmentation pathway of GPE (glycerophosphoryl-ethanolamine).

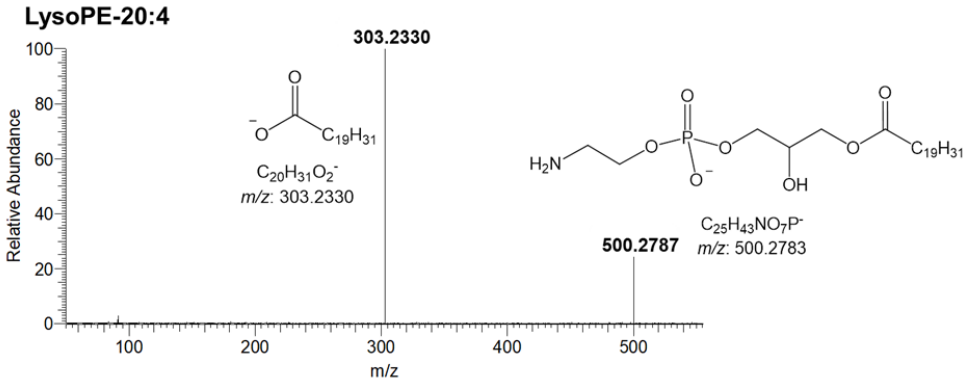

Figure S33. The MS/MS spectrum and the fragmentation pathway of LysoPE-20:4.

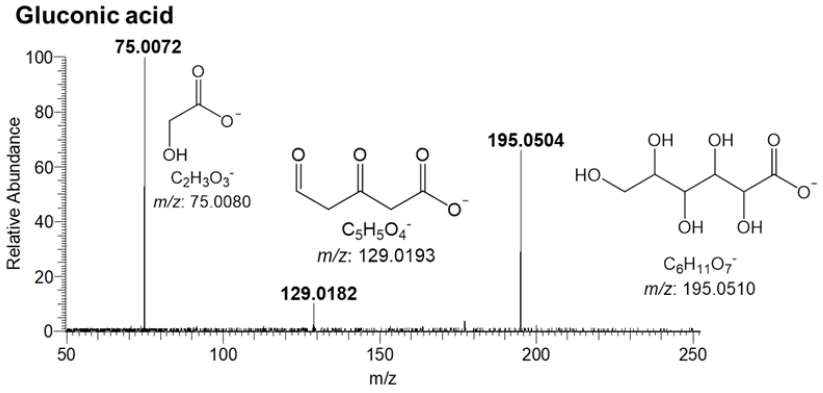

Figure S34. The MS/MS spectrum and the fragmentation pathway of gluconic acid.

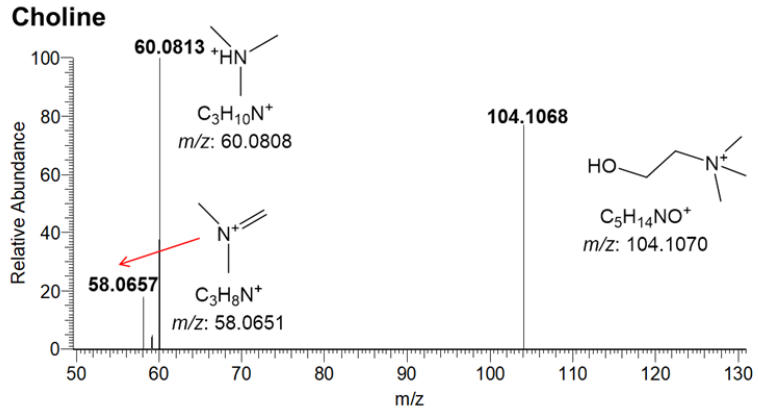

Figure S35. The MS/MS spectrum and the fragmentation pathway of choline.

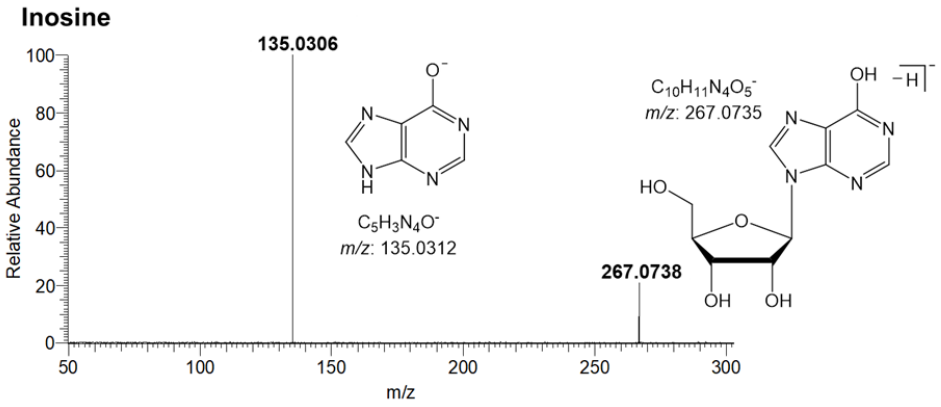

Figure S36. The MS/MS spectrum and the fragmentation pathway of inosine.

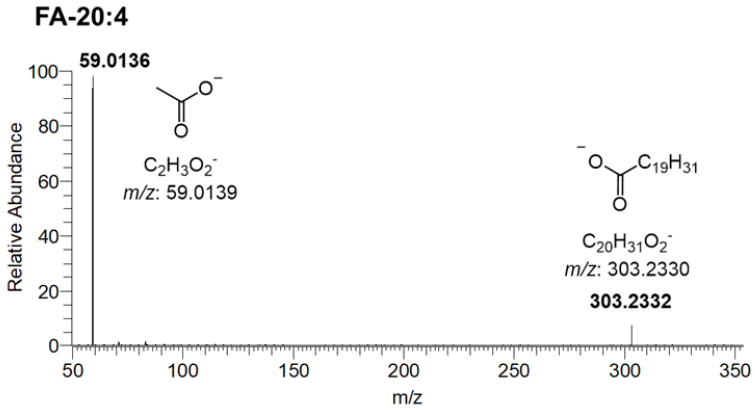

Figure S37. The MS/MS spectrum and the fragmentation pathway of FA-20:4.

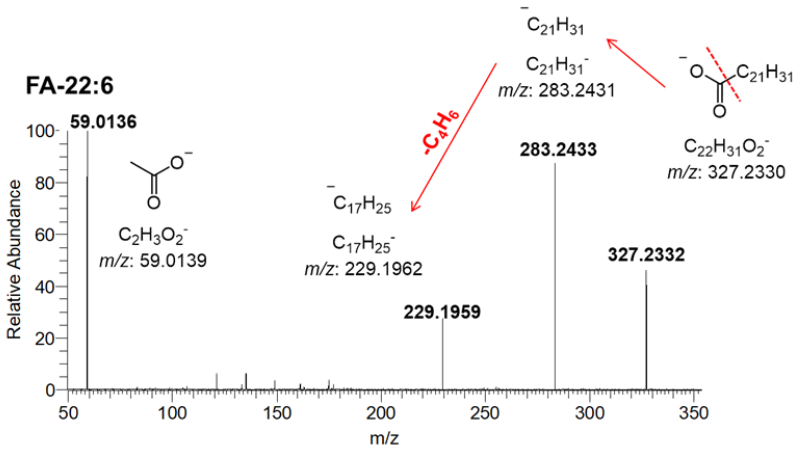

Figure S38. The MS/MS spectrum and the fragmentation pathway of FA-22:6.

Table S1. Screened discriminating metabolites based on AFADESI-MSI data.

Metabolites	Formula	Ion type	Theoretical *m/z*	Measured *m/z*	Relative Error(ppm)	MS image	Relative ion intensity	Metabolic pathway
Proline	$C_5H_9NO_2$	$[M+H]^+$	(+) 116.0706	(+) 116.0704	-1.72	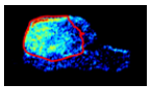	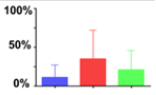	Arginine and proline metabolism
Spermine	$C_{10}H_{26}N_4$	$[M+H]^+$	(+) 203.2230	(+) 203.2228	-0.98	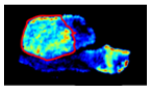	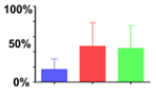	Arginine and proline metabolism
Spermidine	$C_7H_{19}N_3$	$[M+H]^+$	(+) 146.1651	(+) 146.1648	-2.05	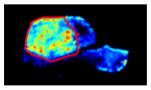	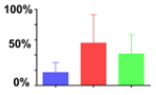	Arginine and proline metabolism
Histamine	$C_5H_9N_3$	$[M+H]^+$	(+) 112.0870	(+) 112.0869	-0.89	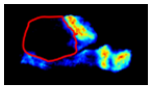	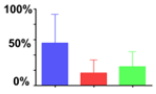	Histidine metabolism
Methyl-histamine	$C_6H_{11}N_3$	$[M+H]^+$	(+) 126.1026	(+) 126.1024	-1.59	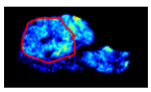	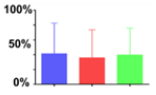	Histidine metabolism
Histidine	$C_6H_9N_3O_2$	$[M-H]^-$	(-) 154.0622	(-) 154.0617	-3.25	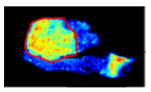	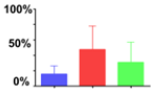	Histidine metabolism
Uracil	$C_4H_4N_2O_2$	$[M-H]^-$	(-) 111.0200	(-) 111.0195	-4.50	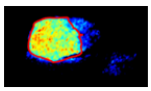	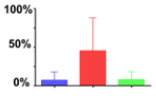	Pyrimidine metabolism
Uridine	$C_9H_{12}N_2O_6$	$[M-H]^-$	(-) 243.0623	(-) 243.0620	-1.23	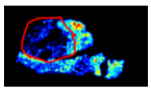	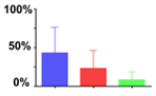	Pyrimidine metabolism
Glutamate	$C_5H_9NO_4$	$[M-H]^-$	(-) 146.0459	(-) 146.0453	-4.11	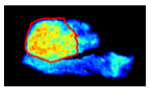	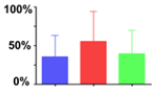	Glutamine and glutamate metabolism
Glutamine	$C_5H_{10}N_2O_3$	$[M-H]^-$	(-) 145.0619	(-) 145.0613	-4.14	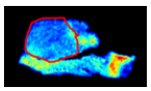	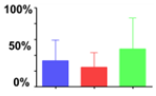	Glutamine and glutamate metabolism
FA-20:4	$C_{20}H_{32}O_2$	$[M-H]^-$	(-) 303.2330	(-) 303.2334	1.32	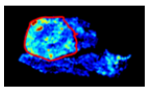	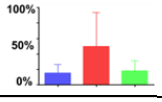	Fatty acid biosynthesis
FA-22:6	$C_{22}H_{32}O_2$	$[M-H]^-$	(-) 327.2330	(-) 327.2335	1.53	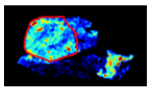	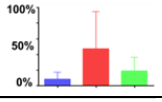	Fatty acid biosynthesis
FA-22:5	$C_{22}H_{34}O_2$	$[M-H]^-$	(-) 329.2486	(-) 329.2492	1.82	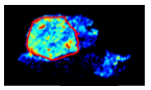	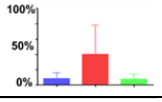	Fatty acid biosynthesis
FA-22:3	$C_{22}H_{38}O_2$	$[M-H]^-$	(-) 333.2802	(-) 333.2807	1.50	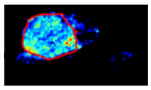	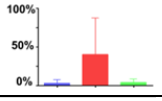	Fatty acid biosynthesis
FA-24:1	$C_{24}H_{46}O_2$	$[M-H]^-$	(-) 365.3425	(-) 365.3430	1.37	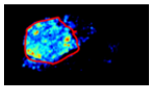	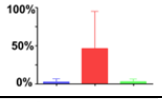	Fatty acid biosynthesis
FA-24:2	$C_{24}H_{44}O_2$	$[M-H]^-$	(-) 363.3272	(-) 363.3272	1.38	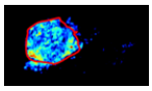	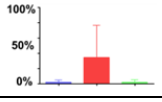	Fatty acid biosynthesis

FA-24:3	$C_{24}H_{42}O_2$	$[M-H]^-$	(-) 361.3116	(-) 361.3116	1.66	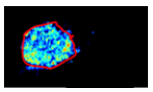	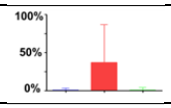	Fatty acid biosynthesis
FA-24:4	$C_{24}H_{40}O_2$	$[M-H]^-$	(-) 359.2958	(-) 359.2958	1.95	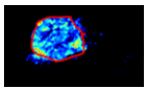	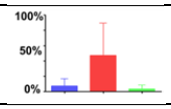	Fatty acid biosynthesis
Glucose	$C_6H_{12}O_6$	$[M+Cl]^-$	(-) 215.0328	(-) 215.0324	-1.86	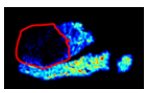	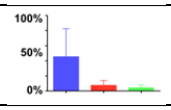	Glycolysis metabolic pathway
Glucose phosphate	$C_6H_{13}O_9P$	$[M-H]^-$	(-) 259.0224	(-) 259.0223	-0.39	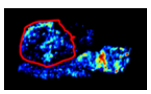	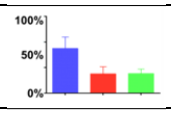	Glycolysis metabolic pathway
Phospho-glyceric acid	$C_3H_7O_7P$	$[M-H]^-$	(-) 184.9857	(-) 184.9851	-3.24	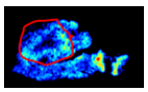	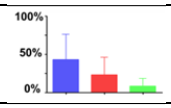	Glycolysis metabolic pathway
Phospho-glycerol	$C_3H_9O_6P$	$[M-H]^-$	(-) 171.0064	(-) 171.0058	-3.51	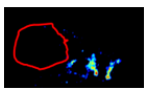	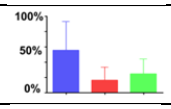	Glycolysis metabolic pathway
Lactic acid	$C_3H_6O_3$	$[M-H]^-$	(-) 89.0244	(-) 89.0240	-4.49	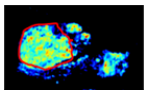	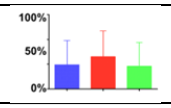	Glycolysis metabolic pathway
Citric/ Isocitric acid	$C_6H_7O_7$	$[M-H]^-$	(-) 191.0197	(-) 191.0188	-4.71	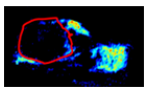	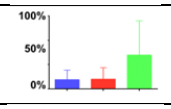	Tricarboxylic acid cycle
Succinic acid	$C_4H_5O_4$	$[M-H]^-$	(-) 117.0193	(-) 117.0188	-4.27	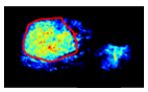	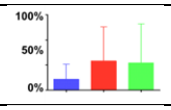	Tricarboxylic acid cycle
Fumaric acid	$C_4H_3O_4$	$[M-H]^-$	(-) 115.0037	(-) 115.0032	-4.35	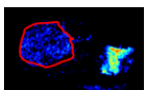	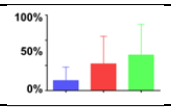	Tricarboxylic acid cycle
Malic acid	$C_4H_5O_5$	$[M-H]^-$	(-) 133.0142	(-) 133.0136	-4.51	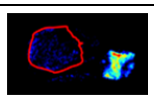	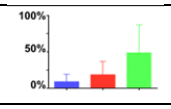	Tricarboxylic acid cycle

■Cancer region, ■Epithelial region, ■Muscular region.

Table S2. Screened potential tumor-associated metabolic enzymes in ESCC.

Enzyme	EC number	Pathway	Related metabolites	Function
PYCR2	EC:1.5.1.2	Arginine and proline metabolism	Proline	Catalyzes the biosynthesis of proline
GLS	EC:3.5.1.2	Alanine, aspartate and glutamate metabolism	Glutamate, Glutamine	Catalyzes the catabolism of glutamine
UPase1	EC:2.4.2.3	Pyrimidine metabolism	Uridine, Uracil	Reversibly converts uridine to uracil
HDC	EC:4.1.1.22	Histidine metabolism	Histidine, Histamine	Stimulates the decarboxylation of histidine to form histamine
FASN	EC 2.3.1.85	FA biosynthesis	Long-chain FAs	Catalyzes the formation of long-chain FAs
ODC	EC:4.1.1.17	Arginine and proline metabolism	Spermine, Spermidine	Involved in amine and polyamine biosynthesis

References

1. Xiang T, et al. (2012) The Ubiquitin Peptidase UCHL1 Induces G0/G1 Cell Cycle Arrest and Apoptosis Through Stabilizing p53 and Is Frequently Silenced in Breast Cancer. *PLoS One* 7(1):e29783.